Accelerated cranial divergence in isolated *Ammospermophilus* lineages: integrating phylogenetic, allometric, and environmental drivers of morphological evolution

Bader Alhajeri[1]

[1]Kuwait University

A - Research concept and design, B - Collection and/or assembly of data, C - Data analysis and interpretation, D - Writing the article, E - Critical revision of the article, F - Final approval of the article

Bader Alhajeri - 0000-0002-4071-0301

Abstract:
Understanding what drives morphological variation is important for both evolutionary biology and conservation. This study explores the factors influencing cranial size and shape variation in antelope ground squirrels (genus *Ammospermophilus*) by combining phylogenetic, allometric, ecological, and geographic perspectives. Geometric morphometric analyses were conducted on 58 cranial landmarks from 157 adult specimens representing four species (seven taxa) from 75 localities. Results show that species identity explains more cranial shape variation than allometry. However, after allometric correction, interspecific shape differences become nonsignificant, suggesting that species distinctions are mainly expressed through allometric effects. Ventral cranial shape shows a greater phylogenetic congruence and better distinguishes taxa (80% classification accuracy) than dorsal shape (66%), suggesting different evolutionary pressures across these cranial regions. Temperature, precipitation, and their seasonality explain >60% of environmental variation across species ranges, with *Ammospermophilus leucurus* uniquely exhibiting strong climate–shape covariation (r-PLS: 0.773-0.802). Geographically isolated taxa show increased morphological differentiation, with the insular *A. l. insularis* and peripheral *A. nelsoni* displaying the most divergent cranial morphologies. These results show that antelope squirrels' cranial evolution is shaped by phylogeny, allometry, ecology, and geographic isolation. The marked morphological and genetic divergence of *A. l. insularis* and *A. nelsoni*, along with their limited ranges, and threatened status, makes them key conservation targets for maintaining phylogenetic diversity in this genus.

Keywords: Sciuridae, Climate, Skull, Geometric morphometrics, Allometry, *Ammospermophilus insularis*.

Received: 2025-05-09
Revised: 2026-02-09
Accepted: 2026-02-09
Final review: 2026-02-02

Short title
Ammospermophilus cranial variation

Corresponding author
Bader Alhajeri
Kuwait University; email: bader.alhajeri@gmail.com

HYSTRIX
the Italian Journal of Mammalogy

Abstract

Understanding what drives morphological variation is important for both evolutionary biology and conservation. This study explores the factors influencing cranial size and shape variation in antelope ground squirrels (genus *Ammospermophilus*) by combining phylogenetic, allometric, ecological, and geographic perspectives. Geometric morphometric analyses were conducted on 58 cranial landmarks from 157 adult specimens representing four species (seven taxa) from 75 localities. Results show that species identity explains more cranial shape variation than allometry. However, after allometric correction, interspecific shape differences become nonsignificant, suggesting that species distinctions are mainly expressed through allometric effects. Ventral cranial shape shows a greater phylogenetic congruence and better distinguishes taxa (80% classification accuracy) than dorsal shape (66%), suggesting different evolutionary pressures across these cranial regions. Temperature, precipitation, and their seasonality explain >60% of environmental variation across species ranges, with *Ammospermophilus leucurus* uniquely exhibiting strong climate–shape covariation (r-PLS: 0.773-0.802). Geographically isolated taxa show increased morphological differentiation, with the insular *A. l. insularis* and peripheral *A. nelsoni* displaying the most divergent cranial morphologies. These results show that antelope squirrels' cranial evolution is shaped by phylogeny, allometry, ecology, and geographic isolation. The marked morphological and genetic divergence of *A. l. insularis* and *A. nelsoni*, along with their limited ranges, and threatened status, makes them key conservation targets for maintaining phylogenetic diversity in this genus.

Keywords

Allometry, *Ammospermophilus insularis*, Climate, Geometric morphometrics, Sciuridae, Skull

Introduction

The genus *Ammospermophilus* Merriam, 1892 (antelope ground squirrels) comprises species named for their affinity to sandy habitats and seed diets (Best et al., 1990c). These rodents inhabit sparsely vegetated arid landscapes such as mountain slopes and sandy regions, where they shelter in self-excavated burrows (Nowak and Paradiso, 1983). Across North America, species cluster in distinct desert regions and exhibit markedly different range sizes, reflecting ecological and geographic divergence (Bowers et al., 2007; Ceballos, 2014). The most widespread species, *A. leucurus*, occupies open shrubby areas with thin soil across the Great Basin, Mojave Desert, and Baja California (Bowers et al., 2007). At the other extreme, *A. insularis* has the narrowest range, being restricted to sandy scrub on Espiritu Santo and Partida islands off Baja California Sur (Ceballos, 2014). The remaining species are of intermediate range: *A. nelsoni* in shrublands and grasslands south of California's San Joaquin Valley, *A. interpres* in rocky Chihuahuan Desert regions, and *A. harrisii* on the plains and valleys of the Sonoran Desert (Bowers et al., 2007; Ceballos, 2014). This ecogeographic diversity—in habitat type, range size, and isolation (insular to widespread)—offers an ideal framework to test drivers of cranial evolution in antelope ground squirrels.

Ammospermophilus contains four (Mammal Diversity Database, 2025), five (McLean et al., 2018; Wilson and Reeder, 2005), or six (Mantooth et al., 2013) species (Fig. 1), with taxonomic sources disagreeing on whether *A. leucurus* represents a single species or should be split into two or three distinct cryptic species. Specifically, *A. insularis* is classified either as a subspecies of *A. leucurus* (e.g., Álvarez-Castañeda, 2007; Mammal Diversity Database, 2025) or as a separate species (e.g., Howell, 1938; Mantooth et al., 2013; Wilson and Reeder, 2005), with Mantooth *et al.* also suggesting the existence of additional cryptic species within the *A. leucurus*

complex. Two recent molecular trees (Mantooth et al., 2013; McLean et al., 2018) (Fig. 1) agree that *A. nelsoni*, *A. harrisii*, and *A. leucurus* (excluding *A. insularis*) form a clade (hereafter 'main clade'), but differ on other phylogenetic relationships. Mantooth *et al.* (2013) identified an unresolved trichotomy involving the main clade, *A. interpres*, and a third clade (*A. insularis* + *A. leucurus* from southern Baja California), with *A. leucurus* in the main clade restricted to populations from northern Baja California and the USA. On the other hand, McLean *et al.* (2018) place *A. interpres* sister to the main clade and *A. insularis* as basal. They further disagree on intraclade affinities: Mantooth *et al.* pair *A. leucurus* with *A. harrisii*, whereas McLean *et al.* recover it as sister to *A. nelsoni* (Fig. 1). In *Ammospermophilus*, as in other rodents, phenotypic traits (particularly skull morphology) have traditionally served for species diagnosis (Howell, 1938), yet the correspondence between cranial morphology and molecular phylogenetic relationships remains largely unexplored.

Past research on *Ammospermophilus* cranial morphology has been mostly taxonomic and qualitative (Belk and Smith, 1991; Best et al., 1990d, 1990b, 1990a, 1990c; Howell, 1938). Broader studies on Sciuridae occasionally include *Ammospermophilus* specimens (e.g., McLean et al., 2018), but none specifically examine the predictors of skull variation within this genus. Therefore, a comprehensive quantitative analysis of cranial variation in antelope squirrels is needed to disentangle its phylogenetic, allometric, ecological, and geographic drivers.

Phylogeny and allometry are well studied drivers of mammalian cranial variation, with morphology being constrained by shared ancestry and predictable size-dependent shape changes (Mitchell et al., 2024). In desert rodents specifically, previous work revealed significant phylogenetic signal and allometric scaling patterns in cranial shape, though their relative influence varies across different taxa (Alhajeri, 2025a, e.g., 2025b; Alhajeri and Steppan, 2025).

'Craniofacial evolutionary allometry' (CREA) describes a common pattern in mammals where larger body size typically corresponds to a longer face (Cardini, 2019). Recently, this allometric trend has been generalized to include increased skull "gracilization" in larger animals, which is often linked to ecological pressures involving bite force and diet (Mitchell et al., 2024). Both allometric patterns exhibit relatively smaller braincases in larger crania, following Haller's Rule, where larger species within a clade possess proportionally smaller brains (Rensch, 1948). *Ammospermophilus* cranial allometry remains understudied, leaving its role in shaping skull morphology unclear. Analyzing deviations from expected allometric scaling may reveal key drivers of cranial shape evolution, including developmental constraints, functional adaptations, and ecological specializations (see Mitchell et al., 2024).

Phylogenetic relationships contextualize *Ammospermophilus* cranial diversity, distinguishing ancestral traits from convergent adaptations to environmental pressures. Phylogenetic signal reflects shared ancestry constraining (morphological) trait variation, where strong signal indicates evolutionary conservatism (often via slow neutral drift or stabilizing selection) and weak signal suggests evolutionary lability driven by divergent or convergent selection (see Blomberg et al., 2003; Kamilar and Cooper, 2013). Detecting phylogenetic signal analytically requires sampling at least 20 species for adequate statistical power (Blomberg et al., 2003). The terms "phylogenetic constraint," "phylogenetic inertia," or "phylogenetic effect" generally refer to the same pattern (see Blomberg et al., 2003; Kamilar and Cooper, 2013) but without implying statistical testing, making them more appropriate for qualitative assessments of morphological–phylogenetic concordance in smaller clades like antelope squirrels.

While ecological pressures may drive convergent cranial evolution in *Ammospermophilus*, such adaptive hypotheses remain largely untested within this genus. The

sole comparative ecological study of antelope squirrels focused on antipredator vocalization–habitat relationships rather than cranial traits (Bolles, 1988). Broader sciurid research links diet, fossoriality, locomotion, and sociality as cranial shape drivers (Bertrand et al., 2021; Cardini and O'Higgins, 2004; Gomes Rodrigues and Damette, 2023; Lu et al., 2014; McLean et al., 2018), while arid-adapted rodents show climate-linked adaptations in the tympanic bullae and nasal passages (e.g., Alhajeri, 2025b; Alhajeri et al., 2025, 2015; Alhajeri and Steppan, 2018). Given *Ammospermophilus*' habitat diversity and demonstrated habitat–skull correlations in other rodents (e.g., Alhajeri, 2025a; Alhajeri et al., 2025; Alhajeri and Steppan, 2025), ecological convergence could uncouple cranial morphology from phylogenetic relationships. The present study addresses the unresolved question of whether cranial variation in antelope squirrels is primarily shaped by phylogenetic history or ecological adaptation.

Geographic isolation, a documented driver of cranial divergence in rodents (e.g., Alhajeri et al., 2025), may similarly shape cranial variation in *Ammospermophilus*, particularly in species with restricted or isolated ranges. Taxa with peripheral (*A. nelsoni*, influenced by "Isolation by Distance") or insular (*A. insularis*, exhibiting "Island Syndrome") distributions experience increased isolation, reducing gene flow and potentially driving cranial divergence through genetic drift and/or local adaptation (see Adler and Levins, 1994; Wright, 1943). Patterns of cranial variation in antelope squirrels may be explained by a combination of these geographic drivers interacting with phylogenetic history and ecological pressures, but the relative influence of each factor remains untested.

The present study investigates cranial shape variation in *Ammospermophilus* through an integrated framework of phylogeny, allometry, ecology, and geography. This variation is quantified via geometric morphometrics, where generalized Procrustes analysis (GPA; Rohlf and

Slice, 1990) removes isometric size to generate shape variables, with allometric effects analyzed separately (see Zelditch et al., 2012). First, I hypothesize that cranial shape aligns with phylogenetic relationships and allometric scaling, predicting morphological similarity among closely related or similarly sized taxa. Second, ecological factors (habitat, climate, diet) are expected to drive cranial convergence among species occupying similar niches, independent of their phylogenetic relatedness. Third, geographic isolation (demonstrated by insular *A. insularis* and peripheral *A. nelsoni*) is predicted to increase cranial divergence through genetic drift and/or local adaptation, consistent with Island Syndrome and Isolation by Distance mechanisms.

Materials and methods

Study taxa

A total of 157 *Ammospermophilus* specimens from all four species were sampled: 50 *A. leucurus* (35 *A. l. leucurus*, 12 *A. l. insularis*, 3 *A. l. cinnamomeus*), 39 *A. nelsoni*, 34 *A. harrisii* (25 *A. h. harrisii*, 9 *A. h. saxicolus*), and 34 *A. interpres* (Appendix 1). The dataset comprises 82 males, 74 females, and one specimen of unknown sex, spanning 75 localities (123 from the United States and 34 from Mexico) (Fig. 2; Data S1). Taxonomy was updated to follow the Mammal Diversity Database (2025), with taxonomic authors detailed in Appendix 1.

Specimens were examined at the American Museum of Natural History (AMNH, New York City), the Field Museum of Natural History (FMNH, Chicago), the Museum of Vertebrate Zoology (MVZ, the University of California, Berkeley), the Florida Museum of Natural History (UF, the University of Florida, Gainesville), and the United States National Museum of Natural History (USNM, Washington, D.C.) (Appendix 1). To minimize the influence of cranial condition and age on the results, only adult crania in the best available condition were selected.

Adult status was determined based on fully erupted cheek teeth and fused parietals, interparietals, and frontals (see Bolles, 1988; Sinitsa et al., 2019).

Locality coordinates were obtained from museum online databases or, when unavailable, determined using Google Maps (Google, 2025) following Alhajeri (2021a) (see Data S1 for details). Localities were mapped in R (R Core Team, 2024) using the rnaturalearth (South, 2017) and ggplot2 (Wickham, 2016) libraries.

Geometric morphometric analysis

Cranial images were captured dorsally and ventrally using a Nikon D3200 digital SLR camera with a 40 mm Micro NIKKOR lens (see Alhajeri, 2019). Each image included 1-mm graph paper for pixel-to-millimeter conversion to estimate centroid size. Using ImageJ (Schneider et al., 2012), 17 dorsal and 41 ventral landmarks were digitized on the left half of each cranium, ensuring even coverage (Fig. 3; Table S1). These landmarks were used in similar rodent studies (Alhajeri et al., 2023; e.g., Alhajeri, 2025b; Alhajeri et al., 2025; Dashti et al., 2022a), excluding those not found in *Ammospermophilus*. For example, standard landmarks like the bregma and lambda are omitted because in most adult *Ammospermophilus* specimens, the interparietals, parietals, and often frontals are completely fused to each other (leaving no visible sutures) forming what resembles a single composite bone (see Bolles, 1988; Sinitsa et al., 2019). In cases where the right half of a cranium was better preserved than the left, I digitally mirrored it across the midsagittal plane before landmark digitization. Only the intact view (e.g., ventral) was digitized if landmarks were missing on the other (e.g., dorsal), yielding complete datasets for geometric morphometric analysis (dorsal: n=149; ventral: n=148) (Data S1).

Landmark coordinates were combined into a single tps file (Rohlf, 2015) and flipped along the y-axis using the function rotate.coords("flipY") in the geomorph package (Adams et al., 2024) to match digitization direction (Fig. 3). Generalized Procrustes analysis (GPA; Rohlf and Slice, 1990) was performed with geomorph::gpagen(Proj=T), superimposing landmarks, and projecting them onto tangent space to produce Procrustes shape coordinates and centroid sizes, with the latter log-transformed for further analyses (Data S1). Using geomorph::plotOutliers(), specimens with large Procrustes distances from species' mean shapes were excluded to minimize effects of cranial condition and digitization errors, reducing the dataset from 170 to 157 specimens after eliminating 13 outliers. All subsequent statistical analyses used nonparametric tests with 999 random permutations (α=0.05).

RRPP-ANOVA and pairwise analysis

Sexual dimorphism in centroid sizes and Procrustes coordinates was tested using the lm.rrpp() function from the RRPP library, which utilizes residual randomization in a permutation procedure (RRPP; Collyer and Adams, 2018). Finding no significant sex effects (see Results), all specimens (males, females, and unknown) were pooled for subsequent analyses.

RRPP models excluding sex treated species as the sole predictor of centroid size, and, for Procrustes coordinates, added centroid size plus its interaction with species to partition shared versus species-specific allometries. F-distribution ANOVA tables were computed for each model, applying hierarchical sums of squares in multifactor Procrustes coordinates analyses to account for unequal sample sizes across species (Langsrud, 2003). Following significant interspecific differences (see Results), RRPP::pairwise() calculated species-pair distances based on mean centroid sizes and Procrustes coordinates (both with and without allometric

adjustments), generating pairwise distances, effect sizes, p-values, and confidence limits via RRPP::summary.pairwise(). Intraspecific pairwise tests were similarly performed on the two most heavily sampled subspecies within *A. harrisii* and *A. leucurus*. Finally, I visualized size differences across taxa with ggplot2 boxplots.

Linear discriminant analysis and allometric scaling

I performed a linear discriminant analysis (LDA) to test the ability of Procrustes coordinates to differentiate taxa. Procrustes coordinates were prepared using geomorph::prep.lda() (specifying the taxon as the sole variable), which projects them onto principal components (PCs) for taxon prediction (Collyer and Adams, 2018). The LDA was then performed via the lda() function from the MASS package (Venables and Ripley, 2002) and classification accuracy was assessed through a leave-one-out cross-validated confusion matrix.

Because species-by-centroid-size interactions were significant in the dorsal Procrustes coordinates model (and marginal in the ventral model; see Results), I explored allometry by visualizing shape–size covariation. Standardized shape scores (RegScore; Drake and Klingenberg, 2008) were derived by regressing Procrustes coordinates on centroid sizes, and analyzed for allometry via geomorph::plotAllometry(method="RegScore"). I fitted species-unique allometry models to allow slope heterogeneity and visualized their divergent trajectories using species-specific regression lines. Extreme shapes (minimum/maximum RegScores) were represented as thin-plate spline (TPS) deformation grids using geomorph::plotRefToTarget(), with the sample mean shape (geomorph::mshape()) as reference and the extreme shapes (geomorph::shape.predictor()) as targets. Landmarks were connected using geomorph::define.links() to improve biological interpretability.

213 213

214 214 *Principal component analysis and mean-shape clustering*

215 215 I performed principal component analysis (PCA) on Procrustes coordinates using
216 216 geomorph::gm.prcomp() to identify major axes of shape variation, plotted PC1 and PC2 scores,
217 217 and depicted extreme shapes as TPS deformation grids (mirroring the RegScore analysis).

218 218 Taxon-mean shapes were computed using geomorph::mshape() followed by GPA
219 219 realignment. Taxon-mean clustering patterns were assessed via UPGMA (unweighted pair group
220 220 method with arithmetic mean) dendrograms (Sneath and Sokal, 1973) derived from Procrustes
221 221 distance matrices from the realignment, using the base R function hclust(method="average").
222 222 UPGMA was chosen because it yielded consistent and reliable results in prior studies involving
223 223 other rodent taxa (Alhajeri, 2025a, 2023, e.g., 2021b; Alhajeri and Steppan, 2025). I generated
224 224 separate dorsal and ventral dendrograms, along with a composite dendrogram based on the
225 225 equally weighted average of their matrices. I further assessed taxon differentiation by estimating
226 226 a 'mean of means' shape for each view—equally weighting each taxon regardless of sample size
227 227 (unlike the sample-wide averages in RegScore and PCA—and visualizing each taxon-mean's
228 228 deviation from this consensus with TPS deformation grids.

229 229

230 230 *Climatic PCA and two-block partial least squares analysis*

231 231 Locality climate data were estimated using 19 WorldClim (version 2) bioclimatic variables (Fick
232 232 and Hijmans, 2017; https://www.worldclim.org/bioclim), downloaded as 2.5-minute raster files
233 233 using the raster package (Hijmans, 2019). Variables were standardized (zero mean, unit
234 234 variance) using the base R function scale() to account for unit differences.

A PCA on these standardized variables yielded PC1-2, together capturing 64.4% of climatic variation, which were visualized in scatterplots. Throughout all visualizations (locality map, RegScore, shape and climate PCA plots), species were differentiated by symbols and subspecies by colors.

The relationship between intraspecific cranial variation and climate was assessed using two-block partial least squares (2B-PLS; Rohlf and Corti, 2000) via geomorph::two.b.pls(). This function evaluates relationships between standardized climate variables, and both logged centroid sizes and Procrustes coordinates, analyzing each species separately (not considering subspecies membership).

Results

Components of variation and classification accuracy

No significant sexual dimorphism was detected in centroid size or Procrustes coordinates in either view (all $p>0.050$), justifying the pooling of males, females, and unsexed specimens. This agrees with Best *et al.* (1990c)., who found minimal cranial differences between sexes in *Ammospermophilus* using linear measurements.

In pooled RRPP analyses, centroid size differed significantly among species in both dorsal and ventral views (both $p<0.050$; $Z=3.17–4.87$; $R^2=0.121–0.878$; Table 1a), and three of six species pairs showed significant pairwise size differences in both views (all $p<0.050$; $Z=2.26–3.64$; Table 2a). In both dorsal and ventral views, boxplots show *A. nelsoni* as the largest, *A. leucurus* and *A. h. saxicolus* as the smallest, and the remaining taxa intermediate in size (Fig. 4). Notably, conspecific subspecies sometimes differ markedly in size (Fig. 4). Pooled cranial shape models revealed even stronger interspecific differences (both $p<0.050$; $Z=7.10–$

9.78; R^2=0.118–0.205; Table 1b). Centroid size significantly influenced shape in both views (both $p<0.050$; Z=3.20–4.01; R^2=0.018–0.021; Table 1b), and a size × species interaction (evidence of species-unique allometries) was significant dorsally ($p<0.050$; Z=2.58; R^2=0.031), and marginal ventrally ($p=0.057$; Z=1.52; R^2=0.021; Table 1b). All six species pairs significantly differed in shape in both views (all $p<0.050$; Z=3.40–6.15; Table 2b), but no pairwise differences remained after accounting for common and unique allometries (all $p>0.050$; Table 2c).

Intraspecifically, *A. h. harrisii* did not significantly differ from *A. h. saxicolus* in size or shape in either view (all $p>0.050$; Table S2). By contrast, *A. l. insularis* was significantly larger than *A. l. leucurus* dorsally ($p<0.050$; Z=2.65; R^2=0.210), but not ventrally ($p>0.050$; Table S2a), and its cranial shape differed in both views (both $p<0.050$; Z=4.81–5.26; R^2=0.177–0.178; Table S2b). Shape LDA classified subspecies more accurately from ventral (80%) than dorsal (66%) data (Table S3). The highest accuracies occurred in monotypic species or those with a single sampled subspecies—*A. interpres* (85–100%) and *A. nelsoni* (79–89%)—and *A. l. insularis* (100% in both views; Table S3). The remaining misclassifications were mainly within species (e.g., *A. h. saxicolus* being misclassified as *A. h. harrisii* and vice versa). Disregarding subspecies and analyzing at the species level increased overall classification accuracy in both views to 71–91%.

Allometric scaling, PCA morphospace, and clustering of mean shapes

TPS deformations at RegScore extremes reveal that increased cranial size is associated with rostral elongation, facial and zygomatic arch expansion, and braincase contraction (Fig. 5). In dorsal view, rostral extension involves the nasals, premaxillae and maxillae, while the occipital region is reduced (Fig. 5a). Ventrally, rostral lengthening mostly involves incisive bones; other

modifications include a narrower palatine fissure, an anteriorly shifted masseteric tubercle, an expanded molar row, and narrowed tympanic bullae and foramina magna (Fig. 5b). In both views, *A. leucurus* shows the steepest allometric trajectory and *A. interpres* the flattest (Fig. 5).

PC1–2 captured 30.9% of dorsal and 33.4% of ventral cranial shape variation (Fig. 6). Despite some overlap in morphospace, taxa form distinct clusters and exhibit greater dispersion in the ventral view than in the dorsal view (Fig. 6). In the dorsal plot, PC1 contrasts specimens with elongated rostra, enlarged faces, flared zygomatic arches, and reduced braincases (e.g., *A. nelsoni* and *A. l. leucurus*) near the minimum against those with opposite patterns (e.g., *A. h. saxicolus* and *A. interpres*) near the maximum (Fig. 6a). PC2 differentiates specimens with widened crania, blunted rostra (shorter nasals and premaxillaries), flared zygomatic arches, and compressed braincases near the minimum from those with converse patterns near the maximum (Fig. 6a). This PC2 variation mostly reflects within-taxon variation rather than intertaxonomic divergence. On the ventral PC1, specimens near the minimum (especially *A. nelsoni*) have shortened nasals, elongated incisive bones, expanded molar rows, flared zygomatic arches, and enlarged tympanic bullae, foramina magna magnum, and braincases, along with compressed rostra, while those near the maximum (e.g., *A. l. insularis* and most *A. interpres*) display the opposite suite of traits (Fig. 6b). PC2 contrasts specimens with broad crania with enlarged zygomatic arches and tympanic bullae (e.g., *A. interpres*) near the minimum from those with converse patterns (e.g., *A. h. harrisii* and somewhat *A. h. saxicolus*) near the maximum (Fig. 6b).

Dorsal (Fig. S2a) and ventral (Fig. S2b) shape dendrograms showed different clustering patterns. Because the ventral dendrogram more closely mirrors the phylogenies in Fig. 1, its clustering is reported below in comparison with the two trees. In the ventral dendrogram, *A. l. cinnamomeus* + *A. l. leucurus* and *A. h. harrisii* + *A. h. saxicolus* form separate clusters, which

are then joined by *A. nelsoni* (Fig. S2b). These three species form a clade in both phylogenetic trees in Fig. 1. *A. interpres* then joins this main cluster (Fig. S2b). In the first phylogeny, *A. interpres* forms its own branch (Fig. 1a), whereas in the second it joins the main clade (Fig. 1b). *A. l. insularis* is the most distal taxon in the ventral dendrogram (Fig. S2b), forming a separate third lineage in Fig. 1a (alongside an unsampled species) and occupying the basal position in Fig. 1b.

The composite dendrogram (Fig. 7), which integrates dorsal and ventral data, resulted in clustering intermediate to the separate dendrograms (Fig. S2) and shows lower congruence with the phylogenies (Fig. 1), instead reflecting overall cranial shape similarity. In this dendrogram, *A. l. insularis* is the first to diverge, its mean-shape characterized by broad rostra (especially the maxilla), enlarged palatine fissures, distinctive zygomatic arches, the smallest tympanic bullae, and a contracted cranial base (Fig. 7). *A. l. cinnamomeus* splits next, showing among the largest rostra (driven by premaxilla expansion despite reduced nasals); considering sparse sampling in this taxon, these patterns should be confirmed when more suitable samples become available. *A. nelsoni* diverges next, characterized by a broad cranium, enlarged zygomatic arches, and the largest tympanic bullae (Fig. 7). Subsequently, *A. interpres* diverges with broad nasals, unflared zygomatic arches, and elongated occipitals. *A. l. leucurus* splits next, followed by the *A. h. harrisii* + *A. h. saxicolus* cluster; all three exhibit cranial shapes intermediate among the sampled taxa, reflecting the genus-typical morphology (Fig. 7).

Climate-associated morphological variation

Climate accounted for 38% of the variance on PC1 and 25% on PC2 (Fig. 8; Table S4). PC1 represents a temperature gradient, with relatively strong negative loadings on Annual Mean

Temperature (BIO1, –0.34), Minimum Temperature of the Coldest Month (BIO6, –0.32), and Mean Temperature of the Coldest Quarter (BIO11, –0.34), with temperature variability measures showing weaker positive loadings: Temperature Seasonality (BIO4, +0.14) and Annual Temperature Range (BIO7, +0.08; Table S4). Negative PC1 scores thus correspond to warm, climatically stable sites, while positive scores indicate cooler, more seasonal climates (Fig. 8). PC2 represents a precipitation gradient, driven mainly by Precipitation of the Wettest Month (BIO13, +0.39), Precipitation of Wettest Quarter (BIO16, +0.37), and Precipitation Seasonality (BIO15, +0.36), with moderate contributions from Annual Precipitation (BIO12, +0.28) and Precipitation of the Warmest Quarter (BIO18, +0.30; Table S4). Negative PC2 values therefore indicate arid, non-seasonal climates and posotove values represent more mesic conditions with higher variability (Fig. 8).

Most taxa overlap in PC1–PC2 climate space (Fig. 8), indicating broadly shared climatic adaptations, though some diverge. Excluding an extreme PC2 outlier in *A. h. saxicolus*, that subspecies still exhibits the widest niche. Both *A. h. harrisii* and *A. l. cinnamomeus* occupy dry, low-seasonality environments: *A. h. harrisii* in warm regions (lower left quadrant), and *A. l. cinnamomeus* across lower quadrants regardless of temperature (Fig. 8). *A. l. insularis* lies at the opposite extreme (upper left), reflecting warm, wet habitats with high precipitation seasonality but low temperature seasonality. *A. l. leucurus* spans intermediate positions with a slight tendency toward drier, non-seasonal conditions (lower quadrants) (Fig. 8). *A. interpres* occurs in cooler, highly seasonal environments (right quadrants) and *A. nelsoni* appears in moderately warm, low-seasonality climates (intermediate-to-left quadrants) (Fig. 8).

The 2B-PLS analysis showed significant covariation between climate and cranial size in all species in both dorsal and ventral views (all $p<0.050$; $Z=1.92–3.07$; r-PLS=0.392–0.576)

except *A. nelsoni* (both p>0.050; Table S5a). By contrast, climate–shape covariation was nonsignificant in all taxa in both views (all p>0.050) except *A. leucurus* (both p<0.050; Z=3.32–4.26; r-PLS=0.773–0.802; Table S5b).

Discussion

Allometric scaling

Species identity accounted for around 6–10 times more cranial shape variation in *Ammospermophilus* than allometry (cf. R^2 in Table 1b), with all six species pairs differing significantly in shape (Table 2b) but only three differing in size (Table 2a). However, when shared and unique allometric components were statistically removed (Table 2c), interspecific cranial shape differences disappeared, a pattern previously reported in other rodents (Alhajeri, 2025a, 2025b, 2021c; Alhajeri et al., 2025; Alhajeri and Steppan, 2025). This suggests that species-specific shape divergence is mainly driven by modifications in allometric scaling trajectories, highlighting allometry's central role in generating interspecific cranial differences (see Marroig and Cheverud, 2005).

Size-related cranial shape changes in *Ammospermophilus* follow an allometric pattern where larger crania show rostral elongation, facial and zygomatic arch expansion, and braincase contraction (Fig. 5). These modifications conform to the aforementioned CREA pattern (Cardini, 2019; Mitchell et al., 2024) and Haller's Rule (Rensch, 1948), and correspond to patterns previously observed in other rodents (Alhajeri, 2025a, 2022, 2021c; Alhajeri and Steppan, 2025; Dashti et al., 2022b; Marcy et al., 2020). Furthermore, these size-related cranial shape changes (Fig. 5) align almost exactly with PC1 of dorsal variation (Fig. 6a), indicating that allometric changes drive the main axis of cranial shape variation in antelope squirrels.

Differences in allometric slopes among *Ammospermophilus* species likely reflect either lineage-specific developmental constraints or adaptive responses to divergent ecological pressures, which together influence how cranial shape scales with size (see Marcy et al., 2020; Wilson, 2013). Species-specific and shared allometric trajectories each explained ~2–3% of cranial shape variation (Table 1b), with *A. leucurus* exhibiting the steepest slope and *A. interpres* the shallowest, while *A. harrisii* and *A. nelsoni*'s slopes were intermediate (Fig. 5). These slope differences may reflect functional adaptations to feeding mechanics, since rostrum elongation and zygomatic arch expansion (Fig. 5) are features that reduce mechanical stress during feeding in rodents and correlate with bite force variation and niche divergence (Cox et al., 2012; Maestri et al., 2016). Even minor divergences in allometric trajectories, such as those observed here, may facilitate divergent functional specialization (e.g., see Tavares et al., 2019), highlighting allometry's role in driving cranial diversity within antelope squirrels.

Phylogenetic congruence

The ventral cranial shape of *Ammospermophilus* exhibits a stronger phylogenetic effect (i.e., aligns more closely with molecular phylogenies) than its dorsal shape (Figs. 1, 6, 7, S2), suggesting differential evolutionary constraints across cranial regions. Ventral PCA (Fig. 6b) reveals broader morphospace dispersion and clearer taxonomic clustering (despite some overlap) than the dorsal PCA (Fig. 6a). This superior discrimination likely reflects the taxonomic value of ventral structures, including the auditory bullae, toothrows, and zygomatic arches, which previous work in sciurids has shown to carry strong phylogenetic effect (Álvarez-Castañeda, 2007; Belk and Smith, 1991; Lu et al., 2014). Early taxonomic work on antelope squirrels relied on size and pelage coloration (Howell, 1938), while later studies showed ventral cranial features

(e.g., auditory bullae, occipitals, zygomatic arches, dental traits) provide more reliable taxonomic markers (Belk and Smith, 1991; Best et al., 1990b, 1990d; Cox et al., 2012). Ventral PC1 clearly separates *A. nelsoni* (characterized by compressed rostra, shorter nasals, elongated incisive bones, flared zygomatic arches, larger molars, and enlarged tympanic bullae and foramina magna) from *A. l. insularis* and *A. interpres* (Fig. 6b), reflecting both deep evolutionary divergence and distinct ecological adaptation. The three principal lineages in this genus that Mantooth *et al.* (2013) identified (Fig. 1a) split during the Miocene–Pliocene desert formation—a division mirrored in the ventral taxon-mean shape clusters (Fig. S2b). Together with Miocene fossil records documenting *Ammospermophilus*' early origins (Belk and Smith, 1991), these results highlight the value of ventral cranial morphology for resolving both the evolutionary history and ecological diversification in this genus.

Dorsal PC2—separating wider crania with blunt rostra, flared zygomatics, and compressed braincases from crania with opposite features (Fig. 6a)—primarily reflects intrataxonomic differences, suggesting lower phylogenetic inertia in dorsal regions. The LDA revealed that ventral cranial shape provides better taxonomic discrimination than dorsal shape (80% vs. 66% classification accuracy), with accuracy improving to 71-91% when analyzed at the species, rather than subspecies, level (Table S3). The difference in phylogenetic congruence between dorsal and ventral views aligns with findings in other rodents: dorsal cranial regions typically respond more readily to ecological pressures (habitat use, feeding behavior), while ventral structures (zygomatic arch, auditory bulla, dentition) remain more developmentally constrained and phylogenetically conserved, though still reflecting some dietary adaptations (Cox et al., 2012; Lu et al., 2014; Maestri et al., 2016; McLean et al., 2018). This suggests

418 ventral cranial features provide more reliable phylogenetic information and should be prioritized
419 in taxonomic and systematic studies of *Ammospermophilus* and possibly other squirrels.
420 Phenotypic clustering of skeletal and vocal traits in *Ammospermophilus* sometimes
421 conflicts with molecular phylogenies, suggesting habitat-driven selection can mask true
422 evolutionary relationships (see Best et al., 1990c, 1990a; Bolles, 1988; Ceballos, 2014; Hafner et
423 al., 1998). That ventral cranial shape clustering (Fig. S2b) mirrors molecular phylogenies (Fig.
424 1), while dorsal shape (Fig. S2a) shows weaker concordance, implies that these regions have
425 responded to distinct ecological or developmental pressures and thus warrant separate analyses.
426 Functional demands can override phylogenetic constraint in certain cranial regions. For
427 example, Cox *et al.* (2012) document repeated parallel adaptations in craniomandibular muscle
428 morphology linked to feeding specialization overpowering phylogenetic history, and Mitchell *et*
429 *al.* (2024) show that strong phylogenetic signal in overall cranial size can mask underlying
430 evolutionary allometry. These cases show that diet-related and size-related pressures may shape
431 crania independently of shared ancestry. Broad comparative studies in Sciuridae show that while
432 phylogeny and allometry set baseline constraints on craniodental morphology, adaptive shape
433 changes in particular lineages and skull regions often diverge from phylogenetic expectations,
434 with the relative influence of phylogenetic, allometric, and ecological drivers varying among
435 clades and regions (see Lu et al., 2014; McLean et al., 2018; Menéndez et al., 2023).
436
437 *Ecological drivers*
438 Considering that temperature and precipitation gradients explain >60% of climatic variation
439 across *Ammospermophilus* (Fig. 8), climate is a likely driver of its cranial morphological
440 diversity. PC1 describes a continuum from warm, stable to cool, variable climates, while PC2

441 ranges from dry, consistent to wet, seasonal conditions (Table S4). This climatic framework
442 allows assessing how environmental pressures shape cranial morphology in this genus, since
443 similar temperature and precipitation gradients correlate with cranial variation in other desert-
444 adapted rodents (Alhajeri et al., 2015; Alhajeri and Steppan, 2018).

445 Geographic variation in body size is a common pattern in several *Ammospermophilus*
446 species (Best et al., 1990c; Ceballos, 2014). This variation often appears as larger size in cooler
447 regions, and lighter pelage (and often enlarged bullae) in more arid regions, indicating that such
448 environmental gradients play a significant role in shaping morphological traits (Belk and Smith,
449 1991; Best et al., 1990b, 1990d). The 2B-PLS analysis confirmed a significant association
450 between climate and cranial size in all species except *A. nelsoni* (Table S5a). This prevalent
451 climate-size trend point to consistent selective pressures (e.g., thermoregulation, resource
452 availability) on morphological variation across *Ammospermophilus* species, as previously
453 observed in other rodents (i.e., “Bergmann’s rule”) (Alhajeri and Steppan, 2016; Fourcade and
454 Alhajeri, 2023). The exception of *A. nelsoni* indicates that species-specific factors can override
455 climatic influences on skull size. Combined with earlier evidence of geographic body size clines
456 in *Ammospermophilus* (Best et al., 1990c; Ceballos, 2014), these findings reinforce
457 environmental gradients as drivers of morphological variation in antelope squirrels.

458 Among *Ammospermophilus* species, only *A. leucurus* exhibited significant covariation
459 between climatic variables and cranial shape, with high r-PLS values (0.773–0.802; Table S5b).
460 As the genus’ most geographically widespread taxon, *A. leucurus* inhabits environmentally
461 heterogeneous regions that expose it to substantial climatic variation (Belk and Smith, 1991;
462 Mantooth et al., 2013), likely driving its increased morphological variability along temperature
463 and precipitation clines. Environmental variation may shape cranial traits via local adaptation,

while subspecies diversity, including the potentially distinct *A. l. insularis*, increases genetic and ecological complexity within the species. These findings suggest that widespread taxa with intraspecific phylogeographic structure may develop stronger climate–shape relationships than those with narrower distributions.

Closely related *Ammospermophilus* species often retain similar ecological and morphological traits—a pattern called phylogenetic niche conservatism that may reflect underlying evolutionary constraints (Blomberg et al., 2003; Kamilar and Cooper, 2013; Mitchell et al., 2024). Although they differ in cranial shape (Fig. 7), the largely overlapping climatic niches of most species (Fig. 8) imply shared ecological tolerances. However, some taxa differ sharply in climate: *A. h. harrisii* and *A. l. cinnamomeus* inhabit dry, stable environments, while *A. interpres* inhabits cooler, seasonally variable habitats (Fig. 8). These climatic differences align with the varied habitats of antelope squirrels—from open rocky areas to juniper woodlands—with some species exhibiting ecological flexibility, while others specialize in specific habitats, the latter of which may drive distinct morphology (Best et al., 1990c, 1990b; Howell, 1938). *A. h. harrisii* and *A. l. cinnamomeus* exhibit larger tympanic bullae and longer, narrower nasals than *A. interpres* (Fig. 7)—likely adaptations to greater aridity, enhancing auditory sensitivity in open habitats and respiratory water conservation, as documented in other desert rodents (Alhajeri and Steppan, 2018; Webster and Webster, 1980).

Ammospermophilus species exhibit broad dietary flexibility that potentially influences their craniodental morphology, with diets varying seasonally and by species to include seeds, fruits, vegetation, insects, and occasional small vertebrates (Belk and Smith, 1991; Best et al., 1990c, 1990d; Bowers et al., 2007; Ceballos, 2014; Howell, 1938; Nowak and Paradiso, 1983). Menéndez *et al.* (2023) classified antelope squirrels as primarily granivorous but with distinct

feeding strategies: *A. harrisii*, *A. interpres*, and *A. leucurus* specialize as dry fruit eaters that crush seeds and nuts (the ancestral squirrel diet), while *A. nelsoni* functions as a mixed feeder, consuming both grasses and seeds/nuts through crushing and grinding processes. In rodents, dietary specialization correlates with craniodental morphology: generalists have intermediate skull shapes, while specialists exhibit more divergent forms (Cox et al., 2012; Maestri et al., 2016; McLean et al., 2018; Menéndez et al., 2023). However, my results reveal relatively subtle differences in cranial structure among *Ammospermophilus* feeding strategies, suggesting stronger non-dietary selective pressures on skull evolution. The absence of pronounced differences in bite-force-related features (rostra, incisors, maxilla, zygomatic arches) (Figs. 6, 7) that typically distinguish dietary specialists in rodents (Maestri et al., 2016; Mitchell et al., 2024) likely reflects substantial dietary overlap among antelope squirrels, as in both feeding strategies, seeds are consumed despite their different classifications (Menéndez et al., 2023). Alternatively, cheek pouch evolution may promote an alternative avenue for niche divergence through size-related differences, since larger pouches can accommodate larger seeds (Best et al., 1990c, 1990d; Nowak and Paradiso, 1983).

Habitat structure may exert a stronger selective pressure on *Ammospermophilus* cranial shape than diet, as clustering based on taxon-mean shapes (Fig. 7) correlates better with habitat-associated vocalization patterns than feeding ecology. Species inhabiting open desert environments (*A. leucurus* and *A. harrisii*) display relatively shorter, smaller rostra and narrower zygomatic arches (Fig. 7) compared to species from closed rocky or prairie habitats (*A. nelsoni*, *A. interpres*, and *A. insularis*) which are more variable (Bolles, 1988). These morphological distinctions likely reflect adaptational responses to soil characteristics, as the loose sandy soils of desert habitats require fewer cranial specializations for digging than the harder soils of prairie or

rocky habitats, which typically require wider zygomatic arches to attach stronger masticatory muscles for incisor-assisted burrowing (see Gomes Rodrigues and Damette, 2023). Cranial evolution in *Ammospermophilus* thus reflects both niche conservatism and divergence, driven by various ecological factors that interact with phylogenetic history and geographic distribution in taxon-specific ways.

Geographic isolation

Geographical isolation appears to accelerate cranial divergence in *Ammospermophilus* taxa, with the Espíritu Santo Island-endemic *A. l. insularis* providing evidence for increased morphological evolution. This island taxon exhibits pronounced cranial and dental divergence from mainland relatives, characterized by larger skull size, a broad rostrum, heavy frontal area, and rudimentary or absent anterior premolars (Álvarez-Castañeda, 2007; Best et al., 1990a; Howell, 1938). Such distinctive morphological traits developed under relatively recent insular isolation (~6,900 years ago) and align with predictions of the Island Syndrome, where isolated populations undergo accelerated morphological change (Adler and Levins, 1994). This morphological distinctiveness corresponds with genetic divergence data that supports elevating *A. l. insularis* to species status (Mantooth et al., 2013).

Unlike mainland *A. harrisii* subspecies that showed no significant cranial differences among them, *A. l. insularis* diverges significantly from its mainland counterpart *A. l. leucurus* in both cranial size (dorsal view) and shape (both views) (Table S2). This island taxon exhibits extreme cranial shape differentiation, occupying a distinctive position along ventral PC1, characterized by longer nasals, shorter incisive bones, smaller molar rows, less flared zygomatic arches, deflated tympanic bullae, smaller foramina magna, and expanded rostra versus reduced

braincases (Fig. 6b). The magnitude of this morphological divergence is evidenced by the 100% classification accuracy in both dorsal and ventral analyses, in contrast to the frequent misclassifications observed among mainland subspecies (Table S3). In the composite dendrogram combining dorsal and ventral mean-shape data, *A. l. insularis* diverges first, distinguished by a broad rostrum, enlarged palatine fissures, uniquely shaped zygomatic arches, and the smallest tympanic bullae (Fig. 7), further supporting its cranial distinction.

Beyond its geographical isolation, *A. l. insularis* occupies a unique ecological niche, characterized by distinctive climatic conditions—warmer, wetter environments with high rainfall seasonality, but low temperature variation (Fig. 8). This ecological distinctiveness, combined with insular isolation, likely accelerates cranial evolution, supporting my third hypothesis that geographic isolation promotes cranial divergence in *Ammospermophilus* through the dual mechanisms of genetic drift and local adaptation. *A. l. insularis* represents an incipient species, displaying classic island-driven adaptations (Adler and Levins, 1994; Álvarez-Castañeda, 2007), with the multiple lines of evidence discussed above (extreme cranial divergence in both size and shape, genetic distinctiveness, and ecological specialization) all supporting this conclusion. Given this comprehensive evidence for differentiation across multiple biological dimensions, *A. l. insularis* merits formal recognition and conservation as a distinct species.

Peripheral isolation has similarly driven pronounced cranial divergence in *A. nelsoni*, despite this species sharing a genetic lineage with *A. leucurus* (Figs. 1, 2). This San Joaquin Valley-endemic exhibits distinctive cranial shape features that cause it to split early from other taxa in the combined dorsal–ventral dendrogram, including broader crania and zygomatic arches, proportionally the largest tympanic bullae, and longer nasal bones—all contrasting with the less distinctive shapes of non-isolated lineages (Fig. 7). This cranial shape differentiation, combined

with larger cranial size, and unique vocal traits, likely resulted from prolonged geographical isolation dating back to the early Pliocene (Best et al., 1990d; Bolles, 1988; Howell, 1938; Mantooth et al., 2013). Notably, insular *A. l. insularis* and peripheral *A. nelsoni* both possess the largest crania among all sampled taxa (Fig. 4), aligning with predictions from the "Island Rule" where geographic isolation promotes morphological divergence regardless of isolation mechanism (Adler and Levins, 1994; Álvarez-Castañeda, 2007). These findings support the view that peripheral isolation accelerates cranial divergence in *A. nelsoni*, likely driven by local adaptation to the San Joaquin Valley's distinctive environment. Parallel divergence patterns in insular and peripheral taxa highlight geographic isolation's central role in generating ecomorphological diversity in *Ammospermophilus*.

Both geographically isolated *Ammospermophilus* taxa face significant conservation challenges, with *A. l. insularis* officially listed as threatened and *A. nelsoni* classified as endangered (Álvarez-Castañeda, 2007; Best et al., 1990a, 1990d; Ceballos, 2014; Hafner et al., 1998; Mantooth et al., 2013). *A. nelsoni* has lost >80% of its historical San Joaquin Valley range and now persists only in small, fragmented populations confined to remnant and marginal habitats (Best et al., 1990d; Hafner et al., 1998). Similarly, *A. l. insularis* faces exceptional vulnerability due to its strict confinement to Espíritu Santo Island, where any habitat disturbance could have severe consequences for this recently diverged taxon (Álvarez-Castañeda, 2007; Best et al., 1990a; Ceballos, 2014; Mantooth et al., 2013). Conservation priority for both taxa is justified by their pronounced genetic, morphological, and behavioral distinctiveness, coupled with their narrow, isolated distributions—characteristics that make them unique components of sciurid phylogenetic diversity (Bolles, 1988; Howell, 1938; Mantooth et al., 2013).

Conclusion

This study shows that *Ammospermophilus*' cranial variation reflects multiple interacting evolutionary forces. Allometric scaling drives species differentiation in patterns similar to those observed in other rodent taxa. Ventral cranial shape is more phylogenetically conserved and provides greater taxonomic resolution than dorsal shape, potentially reflecting distinct functional constraints in different cranial regions. Environmental factors significantly influence morphological variation, with *A. leucurus* showing particularly strong climate-shape relationships, likely reflecting its broad geographic distribution. The enlarged tympanic bullae observed in taxa inhabiting drier environments likely reflect functional adaptations. Geographic isolation appears to accelerate morphological divergence, as evidenced by the distinctive cranial characteristics of both insular *A. l. insularis* and peripheral *A. nelsoni*, highlighting their conservation significance. These results advance our understanding of cranial evolution by revealing how morphological diversification emerges from complex interactions between phylogenetic history, allometric scaling, ecological adaptation, and geographic isolation, with cranial regions responding differentially to these evolutionary pressures.

Data availability

Data produced in this study have been deposited in the supplementary materials (Data S1).

Conflict of interest

The author declares no conflict of interest.

Acknowledgments

602 602 I thank staff at AMNH, FMNH, MVZ, UF, and USNM for assistance during museum visits.
603 603 Kuwait University provided scientific leave (2019-2020) and supported travel to the USNM.
604 604 Kuwait University also approved a 2024-2025 sabbatical, which was crucial for completing this
605 605 work. I also acknowledge the comments of two anonymous reviewers. This research received no
606 606 grant funding.
607 607

608 608 **References**

609 609 Adams, D., Collyer, M., Kaliontzopoulou, A., Baken, E., 2024. geomorph: geometric
610 610 morphometric analyses of 2D and 3D landmark data [WWW Document]. URL
611 611 https://cran.r-project.org/web/packages/geomorph/index.html
612 612 Adler, G.H., Levins, R., 1994. The Island Syndrome in Rodent Populations. Q Rev Biol 69, 473–
613 613 490.
614 614 Alhajeri, B.H., 2025a. Interspecific cranial variation in coarse-haired pocket mice (*Chaetodipus*):
615 615 a geometric morphometric analysis within a phylogenetic framework. Mamm Biol 105,
616 616 449–466. https://doi.org/10.1007/s42991-025-00490-2
617 617 Alhajeri, B.H., 2025b. Cranial variation in species and subspecies of kangaroo rats (*Dipodomys*,
618 618 Dipodomyinae, Rodentia) according to geometric morphometrics. Integr Zool 20, 108–134.
619 619 https://doi.org/10.1111/1749-4877.12824
620 620 Alhajeri, B.H., 2023. Cranial geometric morphometrics of jumping mice (Genera: *Eozapus*,
621 621 *Napaeozapus*, and *Zapus*; Zapodinae, Rodentia): Implications for subspecies conservation. J
622 622 Mamm Evol 30, 713–734. https://doi.org/10.1007/s10914-023-09666-4
623 623 Alhajeri, B.H., 2022. Geometric differences between the crania of Australian hopping mice
624 624 (*Notomys*, Murinae, Rodentia). Aust Mammal 44, 24–38. https://doi.org/10.1071/AM20067
625 625 Alhajeri, B.H., 2021a. A geometric morphometric analysis of geographic mandibular variation in
626 626 the dwarf gerbil *Gerbillus nanus* (Gerbillinae, Rodentia). J Mamm Evol 28, 469–480.
627 627 https://doi.org/10.1007/s10914-020-09530-9
628 628 Alhajeri, B.H., 2021b. Cranial variation in allactagine jerboas (Allactaginae, Dipodidae,
629 629 Rodentia): a geometric morphometric study. Zool Res 42, 182–194.
630 630 https://doi.org/10.24272/j.issn.2095-8137.2020.302

631 631 Alhajeri, B.H., 2021c. A morphometric comparison of the cranial shapes of Asian dwarf
632 632 hamsters (*Phodopus*, Cricetinae, Rodentia). Zool Anz 292, 184–196.
633 633 https://doi.org/10.1016/j.jcz.2021.04.001
634 634 Alhajeri, B.H., 2019. Cranial variation in geographically widespread dwarf gerbil *Gerbillus*
635 635 *nanus* (Gerbillinae, Rodentia) populations: Isolation by distance versus adaptation to local
636 636 environments. J Zool Syst Evol Res 57, 191–203. https://doi.org/10.1111/jzs.12247/
637 637 Alhajeri, B.H., Alaqeely, R., Alhaddad, H., 2025. Geometric morphometrics of silky pocket mice
638 638 (*Perognathus*: Perognathinae: Rodentia) crania reveals new insights into their variation,
639 639 evolution, and taxonomy. Zool J Linn Soc 203, zlae029.
640 640 https://doi.org/10.1093/zoolinnean/zlae029
641 641 Alhajeri, B.H., Hasan, Z., Alhaddad, H., 2023. Cranial differences in three-toed jerboas
642 642 (Dipodinae, Dipodidae, Rodentia) according to recent taxonomic revisions. Curr Zool 69,
643 643 475–490. https://doi.org/10.1093/cz/zoac057
644 644 Alhajeri, B.H., Hunt, O.J., Steppan, S.J., 2015. Molecular systematics of gerbils and deomyines
645 645 (Rodentia: Gerbillinae, Deomyinae) and a test of desert adaptation in the tympanic bulla. J
646 646 Zool Syst Evol Res 53, 312–330. https://doi.org/10.1111/jzs.12102/
647 647 Alhajeri, B.H., Steppan, S.J., 2025. Cranial variation across spiny pocket mice (*Heteromys*,
648 648 *Liomys*) in new phylogenetic and taxonomic perspectives. Zoology 168, 126238.
649 649 https://doi.org/10.1016/j.zool.2025.126238
650 650 Alhajeri, B.H., Steppan, S.J., 2018. A phylogenetic test of adaptation to deserts and aridity in
651 651 skull and dental morphology across rodents. J Mammal 99, 1197–1216.
652 652 https://doi.org/10.1093/jmammal/gyy099
653 653 Alhajeri, B.H., Steppan, S.J., 2016. Association between climate and body size in rodents: A

654 654 phylogenetic test of Bergmann's rule. Mamm Biol 81, 219–225.
655 655 https://doi.org/10.1016/j.mambio.2015.12.001
656 656 Álvarez-Castañeda, S.T., 2007. Systematics of the antelope ground squirrel (*Ammospermophilus*)
657 657 from islands adjacent to the Baja California peninsula. J Mammal 88, 1160–1169.
658 658 https://doi.org/10.1644/06-MAMM-A-065R3.1
659 659 Belk, M.C., Smith, H.D., 1991. *Ammospermophilus leucurus*. Mamm Species 1–8.
660 660 https://doi.org/10.2307/3504191
661 661 Bertrand, O.C., Püschel, H.P., Schwab, J.A., Silcox, M.T., Brusatte, S.L., 2021. The impact of
662 662 locomotion on the brain evolution of squirrels and close relatives. Commun Biol 4.
663 663 https://doi.org/10.1038/s42003-021-01887-8
664 664 Best, T.L., Caesar, K., Titus, A.S., Lewis, C.L., 1990a. *Ammospermophilus insularis*. Mamm
665 665 Species 1–4. https://doi.org/10.1093/mspecies/364.1
666 666 Best, T.L., Lewis, C.L., Caesar, K., Titus, A.S., 1990b. *Ammospermophilus interpres*. Mamm
667 667 Species 1–6. https://doi.org/10.1093/mspecies/365.1
668 668 Best, T.L., Titus, A.S., Caesar, K., Lewis, C.L., 1990c. *Ammospermophilus harrisii*. Mamm
669 669 Species 1–7. https://doi.org/10.2307/3504155
670 670 Best, T.L., Titus, A.S., Lewis, C.L., Caesar, K., 1990d. *Ammospermophilus nelsoni*. Mamm
671 671 Species 1–7. https://doi.org/10.2307/3504314
672 672 Blomberg, S.P., Garland, T.J., Ives, A.R., 2003. Testing for phylogenetic signal in comparative
673 673 data: behavioral traits are more labile. Evolution (N Y) 57, 717–745.
674 674 Bolles, K., 1988. Evolution and variation of antipredator vocalisations of Antelope squirrels,
675 675 *Ammospermophilus* (Rodentia: Sciuridae). Zeitschrift für Säugetierkd 53, 129–147.
676 676 Bowers, N., Bowers, R., Kaufman, K., 2007. Kaufman Field Guide to Mammals of North

America. Houghton Mifflin, Boston, Massachusetts.

Cardini, A., 2019. Craniofacial allometry is a rule in evolutionary radiations of placentals. Evol Biol 46, 239–248. https://doi.org/10.1007/s11692-019-09477-7

Cardini, A., O'Higgins, P., 2004. Patterns of morphological evolution in Marmota (Rodentia, Sciuridae): geometric morphometrics of the cranium in the context of marmot phylogeny, ecology and conservation. Biol J Linn Soc 82, 385–407.

Ceballos, G., 2014. Mammals of Mexico. Johns Hopkins University Press, Baltimore.

Collyer, M.L., Adams, D.C., 2018. RRPP: an R package for fitting linear models to high-dimensional data using residual randomization. Methods Ecol Evol 9, 1772–1779. https://doi.org/doi:10.1111/2041-210X.13029/

Cox, P.G., Rayfield, E.J., Fagan, M.J., Herrel, A., Pataky, T.C., Jeffery, N., 2012. Functional evolution of the feeding system in rodents. PLoS One 7. https://doi.org/10.1371/journal.pone.0036299

Dashti, Z., Alhaddad, H., Alhajeri, B.H., 2022a. Skull variation in populations of the Indian gerbil *Tatera indica* (Gerbillinae, Rodentia) sampled across its broad geographic range. Vertebr Zool 72, 1077–1098. https://doi.org/10.3897/vz.72.e90474

Dashti, Z., Alhaddad, H., Alhajeri, B.H., 2022b. A geometric morphometric analysis of geographic variation in the Cape short-eared gerbil, *Desmodillus auricularis* (Rodentia: Gerbillinae). Mammalia, Mammalia 86, 615–631. https://doi.org/doi:10.1515/mammalia-2022-0019

Drake, A.G., Klingenberg, C.P., 2008. The pace of morphological change: historical transformation of skull shape in St Bernard dogs. Proc R Soc B Biol Sci 275, 71–76. https://doi.org/10.1098/rspb.2007.1169

700 Fick, S.E., Hijmans, R.J., 2017. WorldClim 2: new 1-km spatial resolution climate surfaces for
701 global land areas. Int J Climatol 37, 4302–4315. https://doi.org/10.1002/joc.5086/
702 Fourcade, Y., Alhajeri, B.H., 2023. Environmental correlates of body size influence range size
703 and extinction risk: A global study in rodents. Glob Ecol Biogeogr 32, 206–217.
704 https://doi.org/https://doi.org/10.1111/geb.13622
705 Gomes Rodrigues, H., Damette, M., 2023. Incipient morphological specializations associated
706 with fossorial life in the skull of ground squirrels (Sciuridae, Rodentia). J Morphol 284.
707 https://doi.org/10.1002/jmor.21540
708 Google, 2025. Google Maps. Version 3.59.8 [WWW Document]. URL https://maps.google.com/
709 (accessed 2.16.25).
710 Hafner, D.J., Yensen, E., Kirkland, G.L., 1998. North American rodents: status survey and
711 conservation action plan, SSC Status Survey and Conservation Action Plans. International
712 Union for the Conservation of Nature and Natural Resources, Gland, Switzerland.
713 Hijmans, R.J., 2019. raster: geographic data analysis and modeling [WWW Document]. URL
714 http://cran.r-project.org/package=raster
715 Howell, A.H., 1938. Revision of the North American ground squirrels: With a classification of
716 the North American Sciuridae (North American fauna), First. ed. USDA Bureau of
717 Biological Survey, Washington, D. C.
718 Kamilar, J.M., Cooper, N., 2013. Phylogenetic signal in primate behaviour, ecology and life
719 history. Philos Trans R Soc B Biol Sci 368. https://doi.org/10.1098/rstb.2012.0341
720 Langsrud, Ø., 2003. ANOVA for unbalanced data: use type II instead of type III sums of
721 squares. Stat Comput 13, 163–167. https://doi.org/10.1023/A:1023260610025
722 Lu, X., Ge, D., Xia, L., Huang, C., Yang, Q., 2014. Geometric morphometric study of the skull

723 723 shape diversification in Sciuridae (Mammalia, Rodentia). Integr Zool 9, 231–245.
724 724 https://doi.org/10.1111/1749-4877.12035
725 725 Maestri, R., Patterson, B.D., Fornel, R., Monteiro, L.R., de Freitas, T.R.O., 2016. Diet, bite force
726 726 and skull morphology in the generalist rodent morphotype. J Evol Biol 29, 2191–2204.
727 727 https://doi.org/10.1111/jeb.12937
728 728 Mammal Diversity Database, 2025. Mammal Diversity Database (Version 2.0). Zenodo.
729 729 https://doi.org/10.5281/zenodo.15007505 [WWW Document].
730 730 https://doi.org/10.5281/zenodo.15007505
731 731 Mantooth, S.J., Hafner, D.J., Bryson, R.W., Riddle, B.R., 2013. Phylogeographic diversification
732 732 of antelope squirrels (*Ammospermophilus*) across North American deserts. Biol J Linn Soc
733 733 109, 949–967. https://doi.org/10.1111/bij.12084
734 734 Marcy, A.E., Guillerme, T., Sherratt, E., Rowe, K.C., Phillips, M.J., Weisbecker, V., 2020.
735 735 Australian rodents reveal conserved cranial evolutionary allometry across 10 million years
736 736 of murid evolution. Am Nat 196, 755–768. https://doi.org/10.1101/2020.04.30.071308
737 737 Marroig, G., Cheverud, J.M., 2005. Size as a line of least evolutionary resistance: Diet and
738 738 adaptive morphological radiation in new world monkeys. Evolution (N Y) 59, 1128–1142.
739 739 McLean, B.S., Helgen, K.M., Goodwin, H.T., Cook, J.A., 2018. Trait-specific processes of
740 740 convergence and conservatism shape ecomorphological evolution in ground-dwelling
741 741 squirrels. Evolution (N Y) 72, 473–489. https://doi.org/10.1111/evo.13422
742 742 Menéndez, I., Zelditch, M.L., Tejero-Cicuéndez, H., Swiderski, D.L., Carro-Rodríguez, P.M.,
743 743 Hernández Fernández, M., Álvarez-Sierra, M.Á., Gómez Cano, A.R., 2023. Dietary
744 744 adaptations and tooth morphology in squirrels: Insights from extant and extinct species.
745 745 Palaeogeogr Palaeoclimatol Palaeoecol 629. https://doi.org/10.1016/j.palaeo.2023.111788

Mitchell, D.R., Sherratt, E., Weisbecker, V., 2024. Facing the facts: adaptive trade-offs along body size ranges determine mammalian craniofacial scaling. Biol Rev 99, 496–524. https://doi.org/10.1111/brv.13032

Nowak, R.M., Paradiso, J.L., 1983. Walker's mammals of the world. Volume II. Fourth edition, Walker's Mammals of the World. The Johns Hopkins University Press, Baltimore.

Paradis, E., Schliep, K., 2019. ape 5.0: an environment for modern phylogenetics and evolutionary analyses in R. Bioinformatics 35, 526–528. https://doi.org/10.1093/bioinformatics/bty633/

R Core Team, 2024. R: a language and environment for statistical computing. R Foundation for Statistical Computing, Vienna, Austria [WWW Document]. URL https://www.r-project.org/

Rensch, B., 1948. Histological Changes Correlated with Evolutionary Changes of Body Size. Evolution (N Y) 2, 218–230. https://doi.org/https://doi.org/10.1111/j.1558-5646.1948.tb02742.x

Rohlf, F.J., 2015. The tps series of software. Hystrix 26, 1–4. https://doi.org/10.4404/hystrix-26.1-11264

Rohlf, F.J., Corti, M., 2000. Use of two-block partial least-squares to study covariation in shape. Syst Biol 49, 740–753. https://doi.org/10.1080/106351500750049806

Rohlf, F.J., Slice, D., 1990. Extensions of the procrustes method for the optimal superimposition of landmarks. Syst Biol 39, 40–59. https://doi.org/10.2307/2992207/

Schneider, C.A., Rasband, W.S., Eliceiri, K.W., 2012. NIH Image to ImageJ: 25 years of image analysis. Nat Methods 9, 671–675. https://doi.org/10.1038/nmeth.2089/

Sinitsa, M. V., Pogodina, N. V., Kryuchkova, L.Y., 2019. The skull of *Spermophilus nogaici* (Rodentia: Sciuridae: Xerinae) and the affinities of the earliest Old World ground squirrels.

769 Zool J Linn Soc 186, 826–864. https://doi.org/10.1093/zoolinnean/zly092

770 Sneath, P.H.A., Sokal, R.R., 1973. Numerical taxonomy. Freeman, San Francisco.

771 South, A., 2017. rnaturalearth: world map data from natural earth [WWW Document]. URL
772 https://cran.r-project.org/package=rnaturalearth

773 Tavares, W.C., Pessôa, L.M., Seuánez, H.N., 2019. Changes in Ontogenetic Allometry and their
774 Role in the Emergence of Cranial Morphology in Fossorial Spiny Rats (Echimyidae,
775 Hystricomorpha, Rodentia). J Mamm Evol 26, 575–585. https://doi.org/10.1007/s10914-
776 018-9433-1

777 Venables, W.N., Ripley, B.D., 2002. Modern applied statistics with S. Fourth edition. Springer,
778 New York.

779 Webster, D.B., Webster, M., 1980. Morphological adaptations of the ear in the rodent family
780 heteromyidae. Integr Comp Biol 20, 247–254. https://doi.org/10.1093/icb/20.1.247

781 Wickham, H., 2016. ggplot2: elegant graphics for data analysis. Springer-Verlag New York,
782 New York.

783 Wilson, D.E., Reeder, D.M., 2005. Mammal Species of the World. A Taxonomic and
784 Geographic Reference, Third. ed. Johns Hopkins University Press.

785 Wilson, L.A.B., 2013. Allometric disparity in rodent evolution. Ecol Evol 3, 971–984.
786 https://doi.org/10.1002/ece3.521

787 Wright, S., 1943. Isolation by Distance. Genetics 28, 114–138.

788 Zelditch, M.L., Swiderski, D.L., Sheets, H.D., 2012. Geometric morphometrics for biologists: a
789 primer. Second edition. Academic Press, Massachusetts.

790

Tables

Table 1. ANOVA results for four linear models: (a) centroid size by species (both views) and (b) Procrustes coordinates with centroid size, species, and their interaction as predictors (both views).

Table 2. Pairwise species mean distances with statistics for (a) centroid size, (b) Procrustes coordinates, and (c) Procrustes coordinates adjusted for common and unique allometries.

Figures

Fig. 1. *Ammospermophilus* relationships based on molecular phylogenies from (a) Mantooth *et al.* (2013; six species) and (b) McLean *et al.* (2018; five species). Relationships are shown as simplified cladograms with arbitrary branch lengths. The Mantooth *et al.* cladogram derives from multi-locus analyses (their Figs. 4 and 5), with species not sampled in the present study shown in gray. The McLean *et al.* cladogram is based on their Fig. 1. Cladograms were generated using the R library ape (Paradis and Schliep, 2019).

Fig. 2. Locality map of sampled specimens with species shown by symbols and subspecies by colors. Geographic coordinates are in Data S1. See Fig. S1 for a zoomed-out map. Map generated using ggplot2 and rnaturalearth.

Fig. 3. Cranium of Texas antelope squirrel *Ammospermophilus interpres* (USNM 119910) from San Andres Mountains, New Mexico, showing landmark positions on (a) dorsal and (b) ventral views. Landmark descriptions appear in Table S1.

Fig. 4. Boxplots of centroid sizes for (a) dorsal and (b) ventral cranial views by taxon. Boxes show medians and quartiles, whiskers extend to values ≤ 1.5 × inter-quartile range, and points represent outliers. Boxes are colored corresponding to the color of the most sampled subspecies within each species (matching Fig. 2). Plot created in ggplot2.

Fig. 5. Shape-size covariation scatterplots for (a) dorsal and (b) ventral views. Standardized shape scores (RegScore; Drake and Klingenberg, 2008) are plotted against centroid size. Species are indicated by symbols and subspecies by colors (matching Fig. 2). TPS deformations at axis extremes display shape variation (5× magnified) with connected landmarks to improve interpretability. The species-unique allometry model (shape ~ size × species; Table 1b) allows

different allometric trajectories per species rather than forcing a common slope. Species-specific regression lines are color-coded by the predominant subspecies. Plot generated using geomorph.

Fig. 6. PC1–2 scatterplots of (a) dorsal and (b) ventral Procrustes coordinates. Species are indicated by symbols and subspecies by colors (matching Fig. 2). Variance explained by PC1–2 is indicated. TPS deformations at axis extremes display shape variation (3× magnified) with connected landmarks to improve interpretability. The mean landmark configuration based on all specimens is shown for each view. Plots generated in geomorph.

Fig. 7. UPGMA dendrogram based on the average of dorsal and ventral taxon-mean Procrustes distance matrices. The TPS deformations at tip labels are of taxon-mean shapes compared to the average of all seven taxon-mean shapes (3× magnified with connected landmarks). Tips are color-coded by predominant subspecies (matching Fig. 2). Dorsal views are shown in blue, while ventral views are depicted in green. Plot generated using geomorph and base R libraries.

Fig. 8. PC1–2 scatterplots of climate data with species shown by symbols and subspecies by colors (matching Fig. 2). Variance explained by PC1–2 is shown. Overlapping points (specimens from the same localities with identical climate data) are represented by larger symbols (using a consistent scaling factor). PCA is based on 19 standardized bioclimatic variables (centered, scaled) from WorldClim (version 2; Fick and Hijmans, 2017) described in Table S4 (which also list the PCA loadings). The plot summarizes the main climatic patterns at axis extremes (based on PCA loadings). Plot generated using geomorph.

840 840 **Appendix and supporting information**

841 841 The appendix, supporting tables, figures, and data are provided separately.

842 842

HYSTRIX
the Italian Journal of Mammalogy

Table 1. ANOVA results for four linear models: (a) centroid size by species (both views) and (b) Procrustes coordinates with centroid size, species, and their interaction as predictors (both views).

	df	SS	MS	R^2	F	Z	p
a. Centroid size (log)							
[Dorsal view]							
Species	3	0.035094	0.011698	0.12193	6.7119	3.1701	0.001
Residuals	145	0.252718	0.001743	0.87807			
Total	148	0.287812					
[Ventral view]							
Species	3	0.08258	0.027528	0.2134	13.022	4.8786	0.001
Residuals	144	0.3044	0.002114	0.7866			
Total	147	0.38698					
b. Procrustes shape							
[Dorsal view]							
Size	1	0.002981	0.002981	0.01846	3.1597	3.2002	0.004
Species	3	0.019179	0.006393	0.11875	6.7754	7.1014	0.001
Size × species	3	0.0051	0.0017	0.03158	1.8019	2.5834	0.006
Residuals	141	0.133039	0.000944	0.82374			
Total	148	0.161506					
[Ventral view]							
Size	1	0.003223	0.003223	0.02127	4.016	4.0144	0.001
Species	3	0.031101	0.010367	0.20523	12.9171	9.7821	0.001
Size × species	3	0.003229	0.001076	0.02131	1.3412	1.529	**0.057**
Residuals	140	0.112361	0.000803	0.74146			
Total	147	0.151539					

Notes: df=degrees of freedom; SS=sequential sums of squares for centroid size models and hierarchical sums of squares for Procrustes coordinates models; MS=mean squares; R^2=R-squared values; F=F-values; Z=effect sizes (standard deviates of F sampling distributions); p=p-values based on 999 permutations. RRPP was used to evaluate the fit of each linear model. Ordinary least squares (OLS) were used to estimate model coefficients. All model terms are significant ($p<0.05$), except for one, which was marginally significant is highlighted in bold. These models omit specimens damaged in either view (from the respective view).

HYSTRIX
the Italian Journal of Mammalogy

Table 2. Pairwise species mean distances with statistics for (a) centroid size, (b) Procrustes coordinates, and (c) Procrustes coordinates adjusted for common and unique allometries.

	(a) Size				(b) Shape (no correction)				(c) Shape (correction)			
	d	UCL	Z	p	d	UCL	Z	p	d	UCL	Z	p
I. Dorsal view												
A. harrisii — A. interpres	0.006	0.021	-0.082	0.552	0.014	0.011	2.897	**0.003**	0.014	0.018	-1.073	0.858
A. harrisii — A. leucurus	0.001	0.020	-1.280	0.885	0.017	0.010	4.448	**0.001**	0.017	0.022	-0.693	0.743
A. harrisii — A. nelsoni	0.036	0.021	2.675	**0.001**	0.023	0.010	5.723	**0.001**	0.020	0.027	-1.749	0.960
A. interpres — A. leucurus	0.008	0.020	0.160	0.450	0.021	0.010	5.434	**0.001**	0.021	0.025	-0.555	0.697
A. interpres — A. nelsoni	0.030	0.020	2.261	**0.006**	0.025	0.010	6.104	**0.001**	0.022	0.028	-1.536	0.935
A. leucurus — A. nelsoni	0.037	0.020	2.905	**0.001**	0.014	0.010	3.407	**0.002**	0.013	0.019	-1.269	0.896
II. Ventral view												
A. harrisii — A. interpres	0.001	0.025	-1.864	0.970	0.026	0.011	5.248	**0.001**	0.026	0.030	-0.411	0.649
A. harrisii — A. leucurus	0.003	0.023	-0.945	0.800	0.015	0.010	3.480	**0.001**	0.016	0.019	-0.349	0.625
A. harrisii — A. nelsoni	0.054	0.025	3.174	**0.001**	0.024	0.011	4.734	**0.001**	0.027	0.031	-0.132	0.558
A. interpres — A. leucurus	0.003	0.023	-0.854	0.784	0.020	0.010	4.431	**0.001**	0.020	0.024	-1.042	0.844
A. interpres — A. nelsoni	0.053	0.024	3.264	**0.001**	0.033	0.011	6.153	**0.001**	0.035	0.040	0.053	0.480
A. leucurus — A. nelsoni	0.056	0.023	3.648	**0.001**	0.026	0.010	4.646	**0.001**	0.030	0.033	0.218	0.417

Notes: d=distances between (least squares) means; UCL=95% upper confidence limit for test statistic (one-tailed); Z=effect sizes; p=p-values based on 999 permutations. Significantly different pairs ($p<0.05$) are in bold. Specimens damaged in either view were excluded (from that view). Procrustes coordinates corrected for common and unique allometries indicate comparisons between least squares means with logged centroid size as a covariate that is also interacting with the species factor.

HYSTRIX
the Italian Journal of Mammalogy

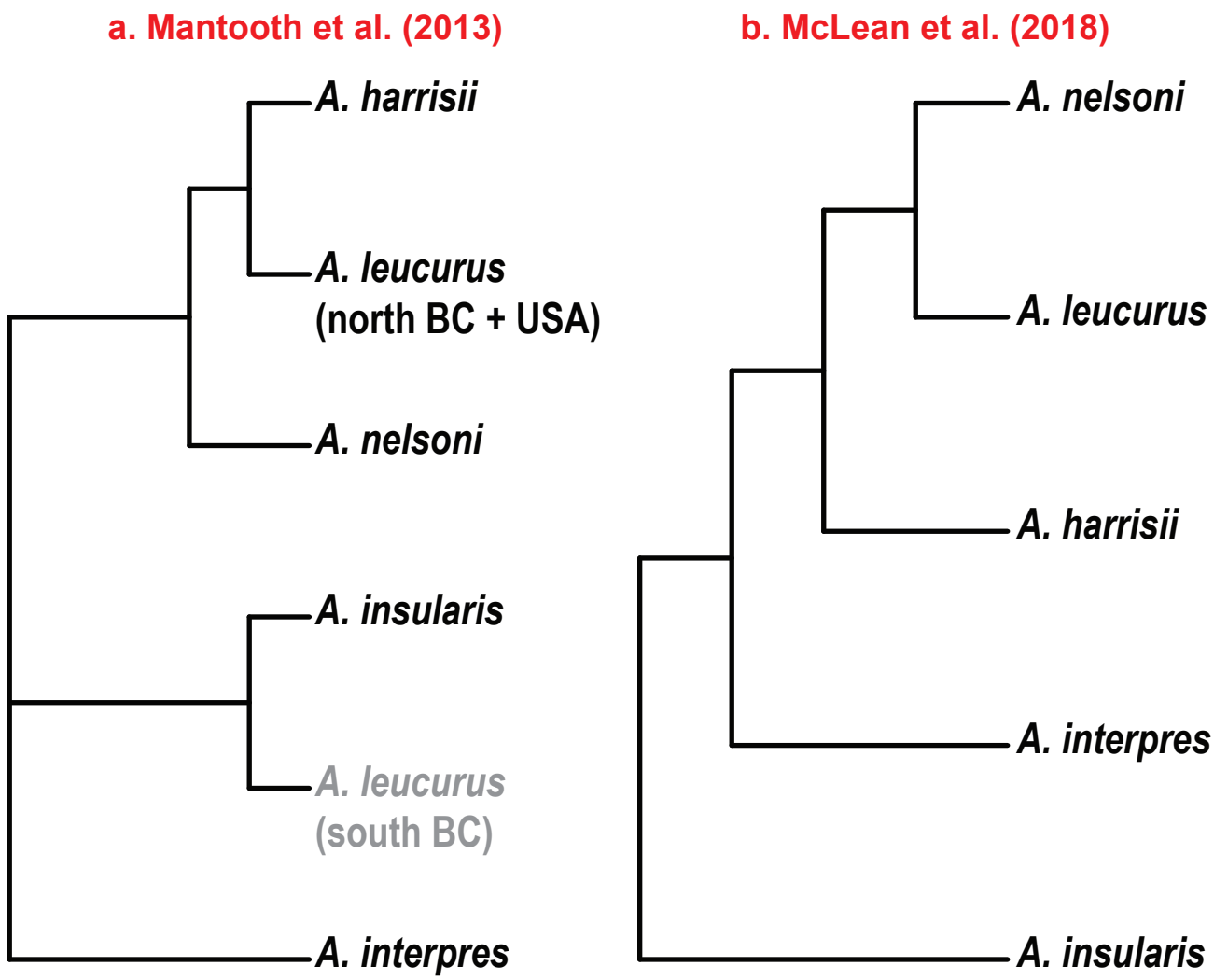

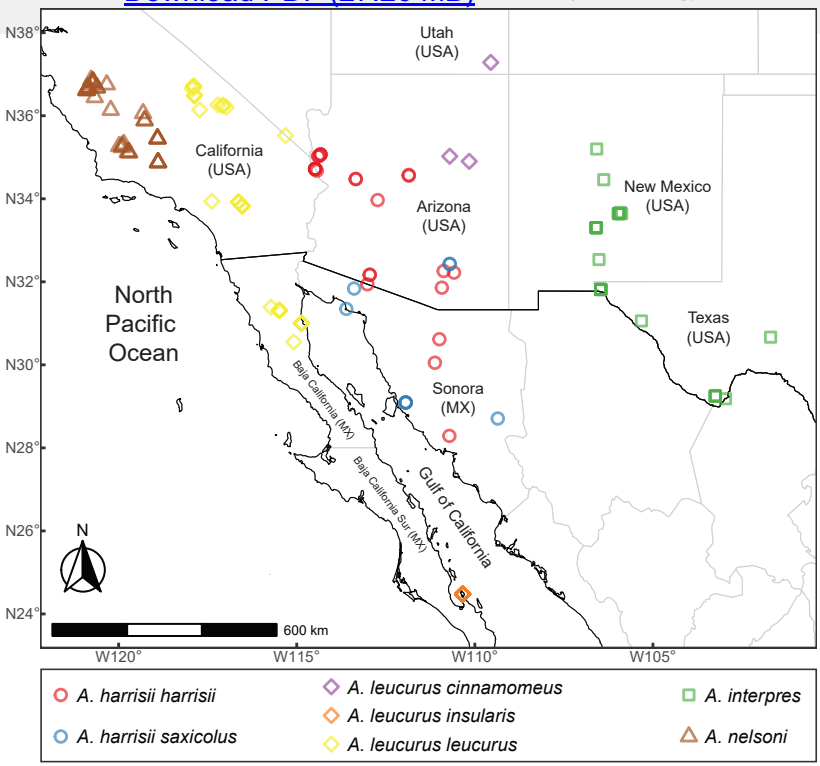

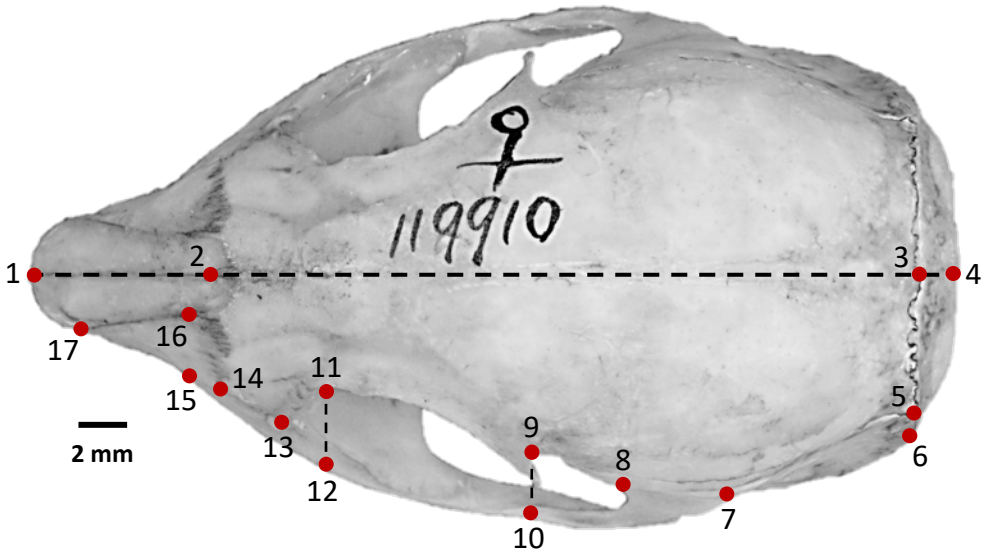

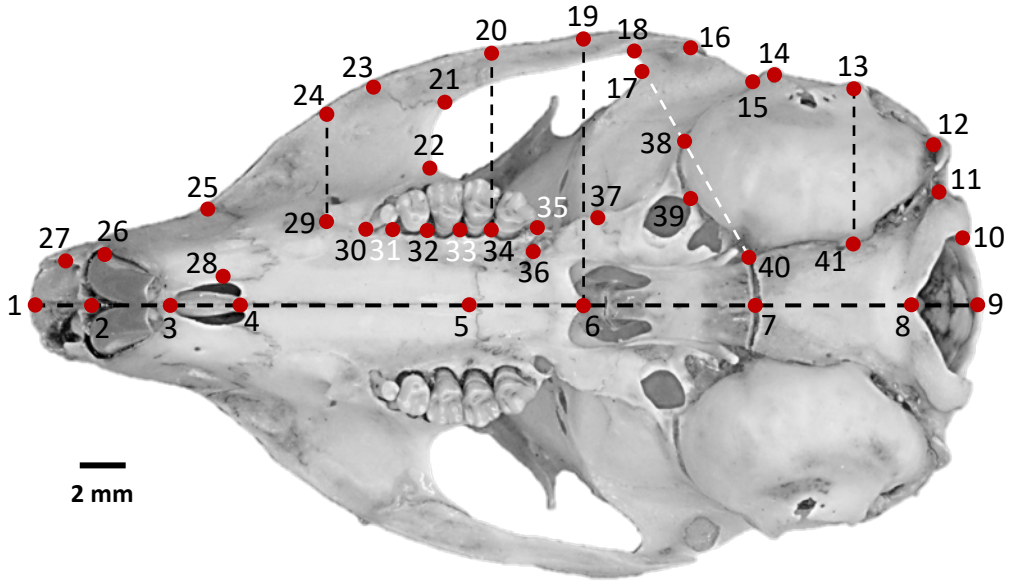

Figure 4

HYSTRIX
the Italian Journal of Mammalogy

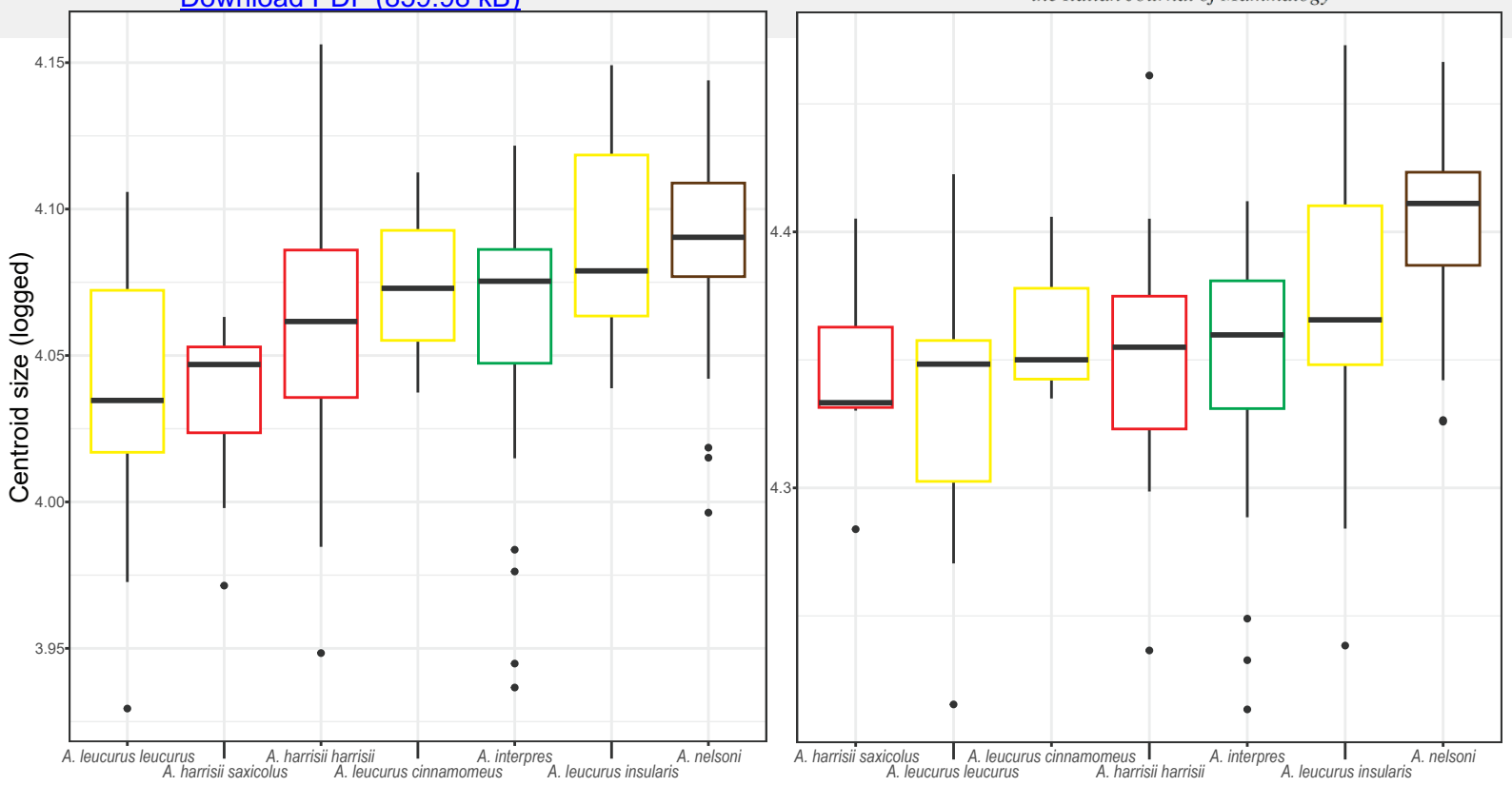

HYSTRIX
the Italian Journal of Mammalogy

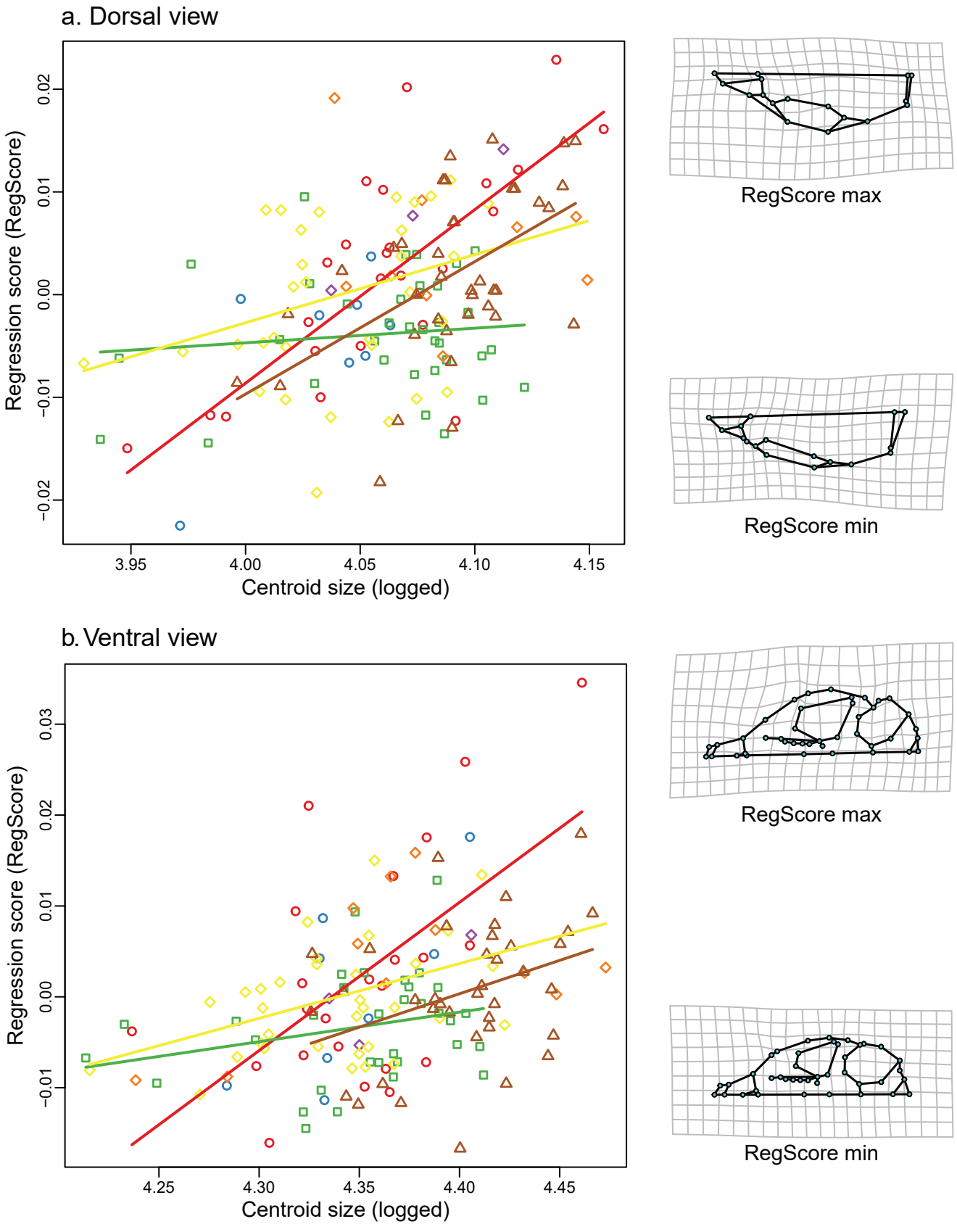

HYSTRIX
the Italian Journal of Mammalogy

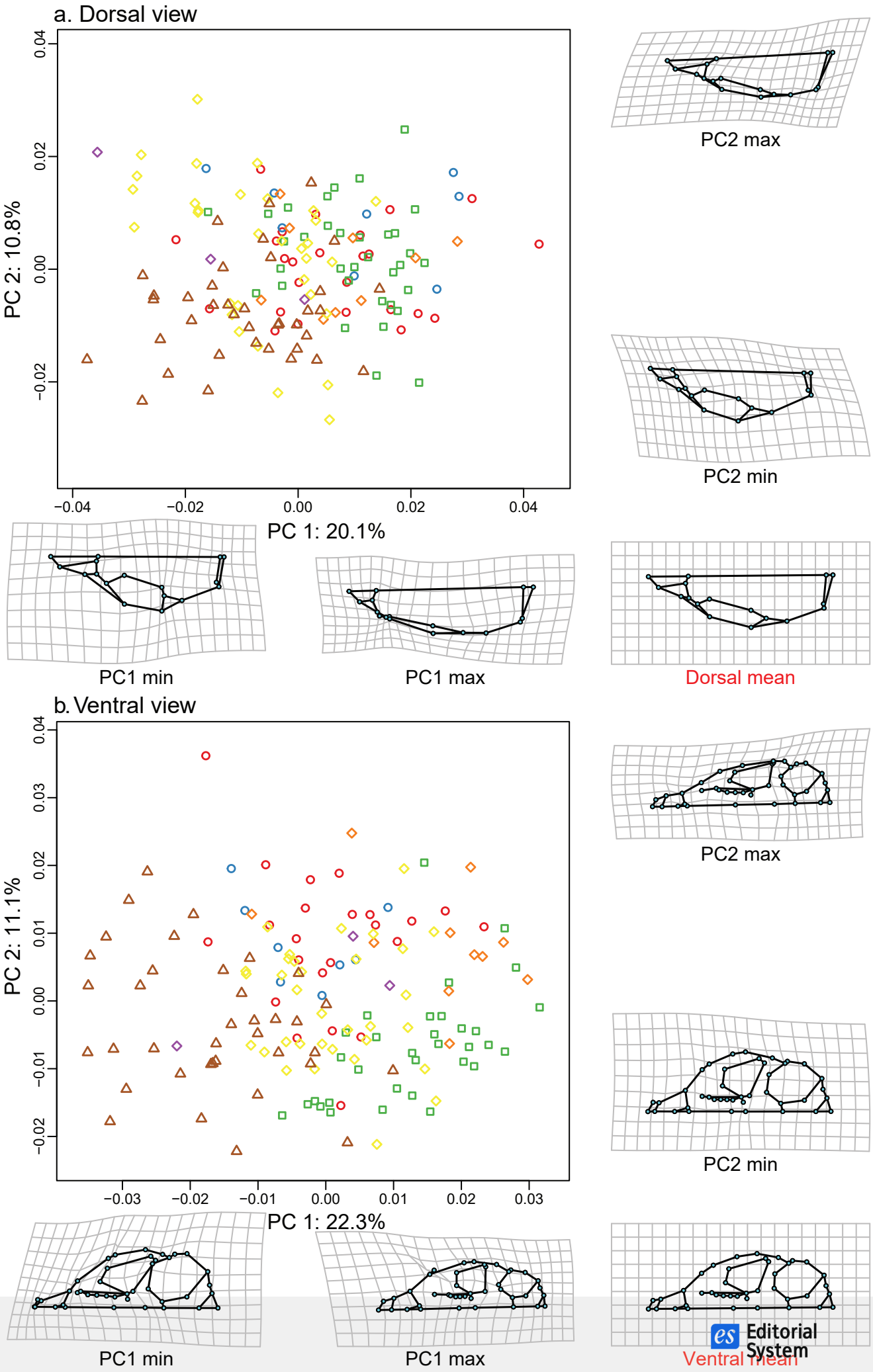

HYSTRIX
the Italian Journal of Mammalogy

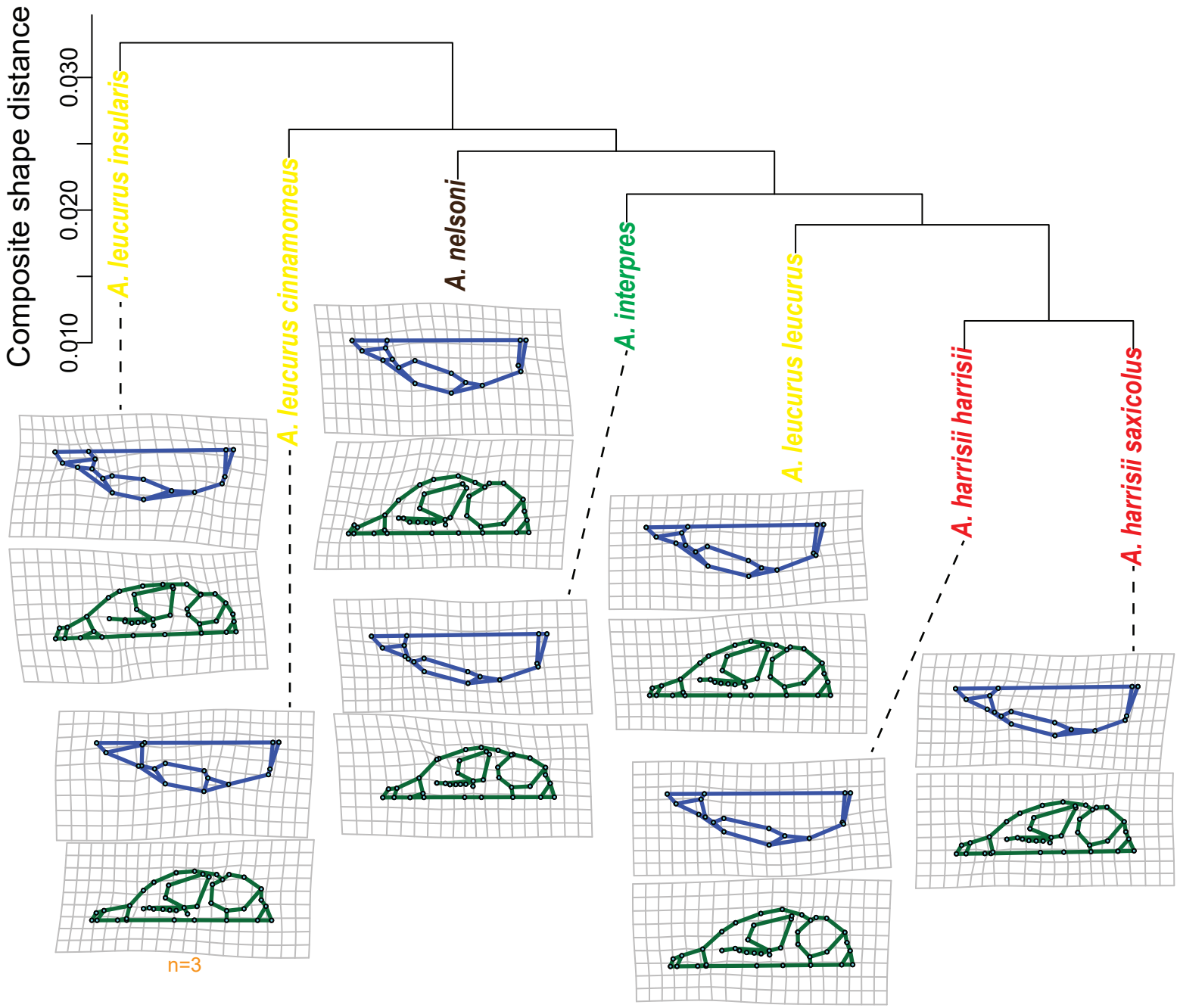

HYSTRIX
the Italian Journal of Mammalogy

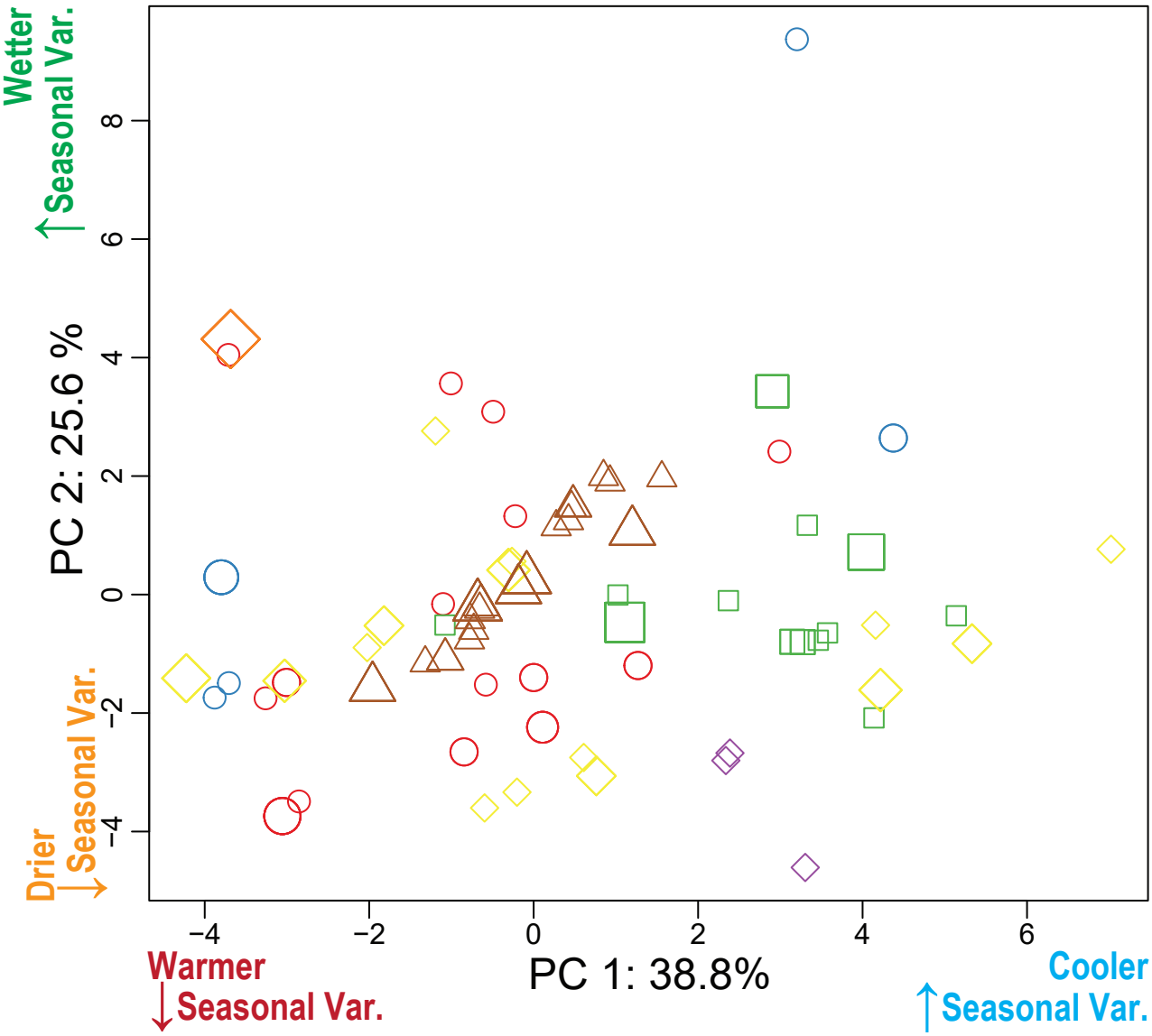

Manuscript body

Download source file (200.42 kB)

Tables

Table 1 - Download source file (18.44 kB)

Table 2 - Download source file (20.2 kB)

Figures

Figure 1 - Download source file (856.86 kB)

Figure 2 - Download source file (27.26 MB)

Figure 3 - Download source file (431.19 kB)

Figure 4 - Download source file (859.98 kB)

Figure 5 - Download source file (981.55 kB)

Figure 6 - Download source file (1.03 MB)

Figure 7 - Download source file (1.09 MB)

Figure 8 - Download source file (882.54 kB)

Supplementary Online Material

File 1 - Download source file (17.06 kB)

File 2 - Download source file (30.6 kB)

File 3 - Download source file (16.47 kB)

File 4 - Download source file (19.16 kB)

File 5 - Download source file (20.47 kB)

File 6 - Download source file (43 kB)

File 7 - Download source file (22.05 MB)

File 8 - Download source file (1.14 MB)

File 9 - Download source file (290.3 kB)